Chemical Geology 290 (2011) 177–188

Contents lists available at SciVerse ScienceDirect

Chemical Geology

journal homepage: www.elsevier.com/locate/chemgeo

Research paper

Response of the U–Pb chronometer and trace elements in zircon to ultrahigh-temperature metamorphism: The Kadavur anorthosite complex, southern India

Ellen Kooijman [a,b,*], Dewashish Upadhyay [a,c], Klaus Mezger [a,d], Michael M. Raith [e], Jasper Berndt [a], C. Srikantappa [f]

[a] Institut für Mineralogie, Westfälische Wilhelms-Universität, Corrensstrasse 24, 48149 Münster, Germany
[b] Department of Earth Science, University of California, 1006 Webb Hall, Santa Barbara, CA 93106-9630, USA
[c] Department of Geology and Geophysics, Indian Institute of Technology, Kharagpur 721 302, India
[d] Institute of Geological Sciences, Universität Bern, Baltzerstrasse 1-3, 3012, Bern, Switzerland
[e] Steinmann Institut, Universität Bonn, Poppelsdorfer Schloss, 53115 Bonn, Germany
[f] Department of Geology, University of Mysore, Manasagangotri, Mysore 570 006, India

ARTICLE INFO

Article history:
Received 5 January 2011
Received in revised form 16 July 2011
Accepted 18 September 2011
Available online 22 September 2011

Editor: L. Reisberg

Keywords:
Zircon
LA-ICP-MS
U–Pb
Anorthosite
UHT
Metamorphism

ABSTRACT

Zircon from quartzites in the contact aureole and wider environs of the Kadavur anorthosite complex, SE India, was studied by laser ablation ICP-MS to assess the response of the U–Pb isotope system and trace element concentrations to ultrahigh-temperature (UHT) contact metamorphism (≥1000 °C). Combined cathodoluminescence imaging and LA-ICP-MS analyses show that zircon grains contain detrital cores, which yield ages between 3.4 Ga and 1.8 Ga and exhibit a large spread in REE concentrations. These cores are associated with one or two rims that provide concordant age populations at 955 ± 16 Ma and 810 ± 7 Ma (2σ) and relatively uniform REE patterns. The older ages of ca. 955 Ma record the imprints of regional early Neoproterozoic metamorphism related to Rodinia assembly. The younger age is interpreted to date anorthosite emplacement and its associated contact metamorphism during a second regional metamorphic episode, coeval with the intrusion of A-type granites in the area. Zircon grains from the country rocks away from the anorthosite show additional rims yielding ages from 590 to 490 Ma corresponding to regional Pan-African tectonometamorphism. The zircon rims are either newly grown domains or represent recrystallized and re-equilibrated parts of precursor zircon. Discordance is only observed in 25% of the detrital cores. These cores have relatively high U concentrations (>400 ppm), which strongly suggests that Pb loss occurred under (U)HT conditions by partial recrystallization (annealing) of zircon that had become metamict. The preservation of old concordant ages and source REE characteristics by the low-U (i.e., weakly to non metamict) detrital cores shows that pristine zircon is extremely robust to thermal disturbance and that its U–Pb systematics can remain unaffected despite multiple (U)HT metamorphic episodes. These observations imply that U–Pb ages in zircon cannot be reset by volume diffusion under any crustal conditions. Disturbance of the U–Pb system in individual zircon crystals or parts thereof can only be achieved by recrystallization of radiation damaged zircon.

1. Introduction

Zircon is a common accessory phase in a wide variety of rock types and strongly fractionates U from Pb during growth (e.g., Silver and Deutsch, 1963) allowing high-precision dating using the U–Pb isotope systems. In metamorphosed rocks, zircon may preserve age information on metamorphic events in newly grown rims or recrystallized older domains (e.g., Schärer et al., 1997; Corfu et al., 2003; Harley et al., 2007). In situ dating of these individual zones, e.g., using laser ablation inductively coupled plasma mass spectrometry (LA-ICP-MS) or secondary ion mass spectrometry (SIMS), are powerful tools for constraining the thermal histories of rocks and the geologic environments of their formation (Harley et al., 2007).

The response of the U–Pb isotope system in zircon to thermal metamorphism depends on several factors such as the pressure and temperature (P–T) conditions, fluid or melt availability, bulk-rock composition, U content and resulting radiation damage, i.e. metamictization (e.g., Silver and Deutsch, 1963; Nasdala et al., 1998), and the mechanisms of zircon formation or re-equilibration. Zircon in metamorphic rocks are either newly grown as a result of mineral reactions (i.e. metamorphic zircon) or have been internally modified by the

* Corresponding author at: Department of Earth Science, University of California, 1006 Webb Hall, Santa Barbara, CA 93106-9630, USA. Tel.: +1 805 350 8121; fax: +1 805 893 2314.
E-mail address: ekooijman@geol.ucsb.edu (E. Kooijman).

0009-2541 © 2011 Elsevier B.V. Open access under CC BY-NC-ND license.
doi:10.1016/j.chemgeo.2011.09.013

metamorphic conditions (metamorphosed zircon). New zircon may nucleate from Zr and Si released during the breakdown of minerals under sub-solidus conditions (Fraser et al., 1997; Pan, 1997) and may also precipitate from fluids (Williams et al., 1996) or melts (Roberts and Finger, 1997) produced during metamorphism. In migmatitic rocks, older zircon grains may dissolve during partial melting and new ones precipitate as overgrowths on older cores (Schaltegger et al., 1999; Vavra et al., 1999; Rubatto et al., 2001). Nemchin et al. (2001) proposed Ostwald ripening as a probable mechanism for textural re-organization of zircon. Pre-existing zircon in rocks may re-equilibrate in response to changing P–T conditions or fluid composition. Geisler et al. (2007) proposed a diffusion reaction process operating at almost any P–T condition to explain the structural recovery of metamict zircon in the presence of a fluid phase. These authors also suggested a melt- or fluid-assisted coupled dissolution–reprecipitation re-equilibration mechanism for crystalline, i.e., non-metamict zircon. In dry, high-temperature (HT) rocks zircon may undergo solid-state recrystallization where structural strain in trace element-rich zircon is dissipated by thermally activated particle and defect volume diffusion (Hoskin and Black, 2000).

The U–Pb ages of zircon often show discordance, commonly attributed to the loss of radiogenic Pb (e.g., Mezger and Krogstad, 1997), e.g., by volume diffusion, leaching by fluids, or recrystallization of metamict grains. Krogh (1982) mechanically abraded partially metamict discordant zircon grains to extract concordant remnants, which indicated that Pb loss in crystalline zircon through volume diffusion was insignificant. Experimental studies have demonstrated that the closure temperature (T_c; Dodson, 1973) of Pb in zircon is high, on the order of 950 to 1000 °C (Lee et al., 1997; Cherniak and Watson, 2001). The resistance of naturally metamorphosed zircon to diffusive Pb loss has also been demonstrated for zircon xenocrysts hosted in felsic magmas (e.g., Gulson and Krogh, 1973; Harrison et al., 1987; Chen and Williams, 1990). However, many studies have questioned the robustness of zircon to diffusive Pb loss during prolonged HT conditions (e.g., Heaman and Parrish, 1991; Ashwal et al., 1999; Flowers et al., 2010), advocating a significantly lower T_c for Pb in zircon than indicated by diffusion experiments.

In order to reliably interpret U–Pb ages of zircon, the causes of discordance need to be understood. The main objectives of our study are to characterize the systematics of U–Pb isotopes and trace elements in zircon exposed to HT regional metamorphism and ultrahigh-temperature (UHT) contact metamorphism, and to investigate zircon crystallization or recrystallization mechanisms under such conditions. For this purpose, we analyzed the U and Pb isotope and trace element compositions of zircon from polymetamorphic quartzites in the contact aureole of the Kadavur massif-type anorthosite in SE India (Fig. 1). These rocks have undergone UHT contact- and regional HT metamorphism enabling the assessment of how prolonged high temperature conditions affect the U–Pb systematics and trace element distribution in zircon. Detrital zircon grains from these quartzites are expected to be U-poor and crystalline, because high-U grains become metamict over time and thus are unlikely to survive sediment transport (e.g., Goldstein et al., 1997). Pristine zircon grains from the rocks allow the evaluation of the significance of diffusive Pb loss through their lattice at (U)HT conditions. The analytical approach combines textural characterization by cathodoluminescence (CL) and

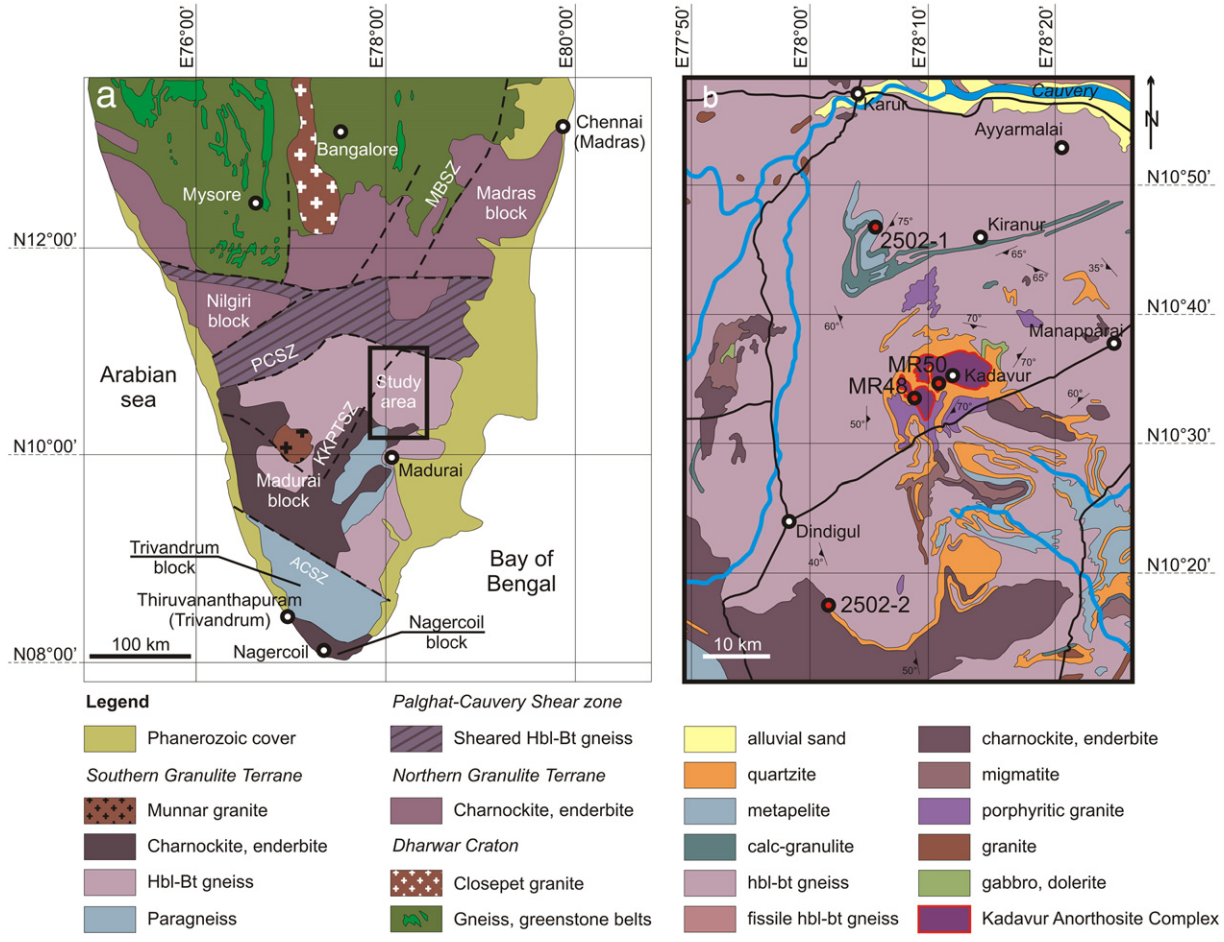

Fig. 1. Geological map of southern peninsular India (a) after Brandt et al. (2011) and the study area (b) after the 1:500,000 geological maps of Tamil Nadu and Pondicherry (Geological Survey of India, 1995). The study area is a part of the Madurai block, which occurs south of the Palghat Cauvery shear zone. Abbreviations are: MBSZ: Moyer-Bhavani shear zone; PCSZ: Palghat Cauvery shear zone; ACSZ: Achankovil shear zone; KKPTSZ: Karur-Kambam-Pianavu-Trichur shear zone.

back-scattered electron (BSE) imaging with spatially resolved U–Pb isotope and trace element analyses using LA-ICP-MS.

2. Geologic setting

The Southern Granulite Terrane (Subramaniam, 1956) in peninsular India (Fig. 1a) represents a large segment of predominantly Archaean and Proterozoic lower continental crust. It is composed of several granulite domains that accreted onto the granite–greenstone Archaean Dharwar craton in the north (Drury and Holt, 1980; Drury et al., 1984; Braun and Kriegsman, 2003). The boundary between the Archaean and Proterozoic domains is commonly thought to be represented by a complex set of ductile shear zones, collectively referred to as the Cauvery Shear Zone system (Drury et al., 1984; Harris et al., 1994; Chetty and Bhaskar Rao, 2006; Rajesh and Chetty, 2006). The Palghat Cauvery Shear Zone represents the southern extremity of this vast east–west network of shear zone systems (Fig. 1a). Several studies have documented evidence for multiple tectonothermal events in the Southern Granulite Terrane over a protracted time period between the Archaean and the late Neoproterozoic (Harris et al., 1994; Bartlett et al., 1998; Braun and Kriegsman, 2003; Santosh et al., 2005). The earliest of these at ca. 2.52 Ga (Baskar Rao et al., 1996; Chetty et al., 2003; Ghosh et al., 2004) produced a crystalline basement, which was overlain by a cover sequence of shallow-marine sediments (quartzites, calc-silicate rocks, and metapelites) deposited during the Mesoproterozoic. In the Madurai Block (Fig. 1a), early Neoproterozoic ages (ca. 0.9 Ga) have been reported from cores of monazite and attributed to HT metamorphism related to the assembly of the supercontinent Rodinia (Braun and Appel, 2006). The basement-cover composite terrane was intruded by massif-type anorthosites and Rapakivi-type granites at ca. 0.8 Ga (S. Brandt, pers. communication; own unpublished data) during a HT regional metamorphic event. Further extensive tectonometamorphic reworking of the Southern Granulite Terrane occurred during the late Neoproterozoic (ca. 0.5 Ga) Pan-African orogeny, which marked the assembly of the supercontinent Gondwanaland (e.g., Harris et al., 1994; Jayananda et al., 1995; Meissner et al., 2002; Santosh et al., 2003). In this event, the areas to the south of the Palghat Cauvery Shear Zone underwent high-temperature metamorphism (Raith et al., 1997; Braun and Kriegsman, 2003; Santosh and Collins, 2003). In the area of Ayyarmalai, northeast of the Kadavur anorthosite complex, two distinct Pan-African age clusters of 615 ± 11 and 529 ± 9 Ma have been obtained by U–Pb dating of zircon (Raith et al., 2010). The older age is related to HT metamorphism associated with extensive magmatism in the Southern Granulite Terrane (Braun and Kriegsman, 2003), whereas the younger age is ascribed to the main phase of high-temperature metamorphism, deformation and anatexis during the Pan-African orogeny (Raith et al., 2010).

3. Sample petrography

Samples were selected from four different locations in and around the Kadavur anorthosite complex, located in the northern part of the Southern Granulite Terrane, south of the Palghat Cauvery Shear Zone (Fig. 1). One quartzite was sampled from a roof pendant within the anorthosite complex (sample 50MR). The second quartzite sample (48MR) was collected from the proximal contact aureole of the intrusion about 600 m from the contact. Two samples were collected from the country-rock supracrustal sequence and include a quartzite (2502–2) taken ca. 20 km to the south of the anorthosite locality and a metapelite (2502–1) from ca. 20 km to the north (Fig. 1b).

Sample 50MR (N 10° 34.380′ E 78° 10.340′) comes from a small isolated quartzite hillock within the southern part of the anorthosite complex, which forms a roof pendant or erosional remnant of the former quartzite roof of the complex (Fig. 1b). The sample site is estimated to lie only a few meters above the anorthosite contact. The quartzites are dark brown-gray. In thin section, they show an inequigranular-interlobate fabric of strain-free quartz grains with local development of polygonal domains (Fig. 2a). Ilmenite and minor magnetite occur as randomly oriented grains. These textures are evidence of extensive static recrystallization, commonly seen in rocks from contact metamorphic aureoles. The quartz has inclusions

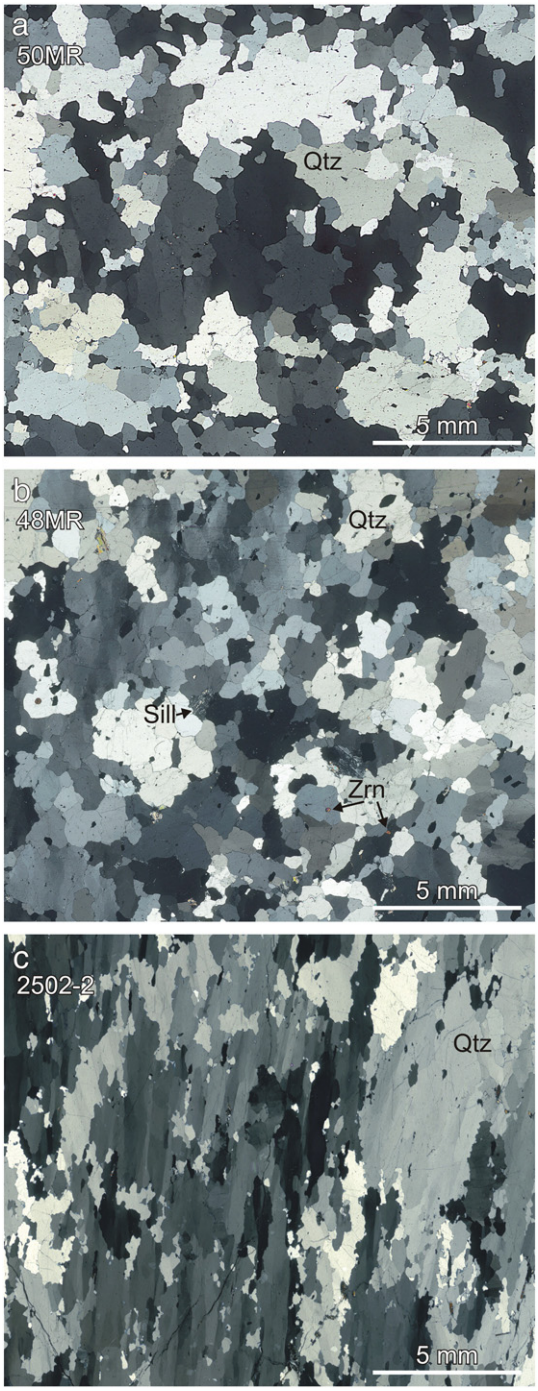

Fig. 2. Photomicrographs (crossed polarizer) illustrating the textural characteristics of roof pendant quartzite (a, 50MR), quartzite in the proximal contact aureole of the anorthosite (b, 48MR), and quartzite from the country rock outside the anorthosite contact aureole (c, 2502–2). Sample 50MR (a) consists of porphyritic coarse aggregates of interlobate to amoeboid quartz grains, which reflect relatively advanced static recrystallization, related to UHT contact metamorphism, overprinting a relict foliation. Static recrystallization is also widespread in the contact-metamorphic quartzite (b), which shows a coarse grain size and random orientation. The country rocks away from the anorthosite locality (c), preserve a well developed foliation defined by large elongate and flattened quartz grains and sillimanite needles. Static recrystallization is only incipient producing just a few coarser grains with lobate grain boundaries.

of randomly oriented minute hexagonal blades of intergrown hematite and ilmenite, interpreted to be exsolution features. Locally, some grains have euhedral carbonic inclusions along planar arrays and abundant trails of predominantly multiphase H_2O–CO_2 inclusions. The latter indicate localized fluid infiltration from a thick pegmatite dyke that occurs west of the exposure.

Sample 48MR was collected from a quartzite ridge in the contact aureole of the anorthosite (N 10° 33.477′ E 78° 09.463′, Fig. 1b). The quartzites preserve a relict foliation defined by stretched quartz grains and well aligned grains of kyanite, sillimanite and ilmenite, which has been largely replaced by an inequigranular-lobate mosaic of strain-free quartz grains (Fig. 2b). The relict quartz grains host trails of monophase carbonic inclusions, most of them having well-defined negative crystal forms. The recrystallized grains are free of fluid inclusions. Kyanite occurs in similar textural relations as sillimanite and shows retrograde alteration to fine-grained micaceous aggregates. Locally, coarser sheets of secondary white mica appear to have grown at these sites.

Sample 2502–2 was collected from the middle part of a thick sequence of quartzites exposed in the Sirumalai Ghats, ca. 20 km to the south of the anorthosite (N 10° 18.785′ E 78° 12.404′, Fig. 1b). The sequence is characterized by an upward gradation from fine-grained quartzite interbanded with fine sillimanite- and biotite-rich layers, through broader bands of medium-grained quartzite to thick bands of very coarse-grained quartzite. Sample 2502–2 has a pronounced foliation defined by large elongate and flattened dynamically-recrystallized quartz grains (Fig. 2c) that include lineation-parallel sillimanite needles as well as boudinaged platy minerals of the hematite–ilmenite group. In contrast to quartzites from near the anorthosite intrusive, there is only little evidence for static recrystallization overprinting the strong schistosity in this sample (Fig. 2c).

Sample 2502–1 was collected from an outcrop of folded metapelites, quartzites, and calc-silicate rocks (N 10° 45.953′ E 78° 05.647′, Fig. 1b), ca. 20 km north of the anorthosite. The rock is a bt + sill + Kfs + crd + qtz + pl + hem ± ky bearing metapelite having a faint compositional banding defined by alternating aluminous and quartzo-feldspathic layers. The aluminous layers comprise polycrystalline sillimanite aggregates (pseudomorphic after porphyroblastic kyanite), cordierite grains replacing sillimanite and biotite, perthitic feldspar, minor quartz, hematite, and magnetite. The quartzo-feldspathic layers are composed of weakly-aligned subhedral biotite grains in granoblastic to interlobate aggregates comprising perthitic feldspar, quartz, and minor plagioclase. The rock contains folded quartz segregation veins with aluminous selvages representing an early foliation defined by the assemblage bt + ky + Kfs + qtz + hem. This foliation is refolded into shallow-plunging open folds. Profuse growth of cordierite at the expense of biotite and aluminosilicate occurred after kyanite was pseudomorphed by polycrystalline sillimanite. The lack of any evidence for melting suggests that cordierite formed via the model dehydration reaction bt + sil + qtz → crd + Kfs + V, which occurs at P–T conditions of <5 kbar and >800 °C (e.g., Spear and Cheney, 1989; Spear, 1999).

4. Analytical methods

Zircon grains were separated from the samples by crushing, followed by magnetic and heavy liquids separation. Representative grains were handpicked under a binocular microscope, taking care to include all sizes and morphologies. For each sample approximately 150 grains were selected and mounted on one inch epoxy disks. These were polished to approximately half the thickness of the grains and internal structures were imaged by CL and BSE techniques using a JEOL JXA-8900 M Superprobe at the Institut für Mineralogie, Westfälische Wilhelms-Universität, Münster. The U–Pb isotope and trace element analyses were performed using a Thermo-Finnigan Element2 sector field ICP-MS coupled to a New Wave UP193HE ArF Excimer laser system at the same institute.

The U–Pb analyses and data reduction were largely carried out following the method of Kooijman et al. (in press). The operating conditions for the laser and the ICP-MS are listed in Table 1. A laser spot size of 12, 25 or 35 μm was used depending on the width of the analyzed zircon zones. The reference zircons were analyzed using a spot size of 25 μm. All spots were pre-ablated by three laser pulses using a 45-μm spot size to remove possible surface common Pb introduced during sample handling. External standardization was done by bracketing groups of five unknowns with two measurements of the GJ-1 reference zircon (Jackson et al., 2004). The raw data were processed offline using an in-house Excel® spreadsheet. The $^{207}Pb/^{206}Pb$ and $^{206}Pb/^{238}U$ were carefully monitored to exclude anomalous parts of the signal related to inclusions or different age zones. Correction for common Pb was done using the two-stage terrestrial Pb evolution model by Stacey and Kramers (1975) if the contribution of the estimated common ^{206}Pb to the total measured ^{206}Pb exceeded 1%. The $^{208}Pb/^{232}Th$ was not measured, because of large analytical errors associated with the ratio. Moreover, measuring additional isotopes using a single-collector ICP-MS leads to larger uncertainties on the other ratios due to longer scanning times. Measurements of the 91500 standard zircon (Wiedenbeck et al., 1995) as unknowns gave an external reproducibility (2σ, $n = 34$) of 2.5% for $^{206}Pb/^{238}U$ and 3.5% for $^{207}Pb/^{206}Pb$. All uncertainties are reported at the 2σ-level. The U contents were estimated relative to the GJ-1 reference. Concordia diagrams were constructed using Isoplot 3.00 (Ludwig, 2003). The U–Pb isotope and age results are listed in Appendix A.

Trace elements were analyzed in some zircon grains of samples 50MR and 48MR adjacent to spots where the U–Pb dating was done in the same CL zone. The same LA-ICP-MS set-up was used, but ablation parameters were 5 Hz and ca. 9 J/cm^2. Correction for instrumental drift was done by bracketing groups of five unknowns with two measurements of the NIST612 glass calibration standard using GeoReM preferred values (MPI, Mainz, Germany, version 11/2006). Concentrations were calculated using GLITTER software (Griffin et al., 2008). The ^{29}Si content, which was calculated from the stoichiometry of zircon, was used as an internal standard. The results are listed in Appendix B. The precision was usually better than 10% depending on the element concentration. Analyses with anomalously high LREE contents possibly related to the presence of inclusions were discarded. The accuracy was monitored by analyzing the 91500 zircon standard (Wiedenbeck et al., 1995) as an unknown. The average concentration determined for each element was usually within error (2σ) of the preferred values for this standard (last two rows of Appendix B). The U concentrations presented in Appendix A are based on direct comparison of count rates with the GJ-1 reference zircon to provide estimates for all samples. Both this approach as well as U concentration analysis using an internal standard were applied to

Table 1
LA-ICP-MS details and operating parameters.

Laser ablation system		ICP-MS	
Model	New Wave Research UP193HE	Model	Element2, ThermoFinnigan
Type	Excimer	Type	Magnetic sector field
Wavelength	193 nm	Forward power	1330 W
Spot size	12, 25 or 35 μm	Scan mode	E-scan
Repetition rate	10 Hz	Scanned masses	202, 204, 206, 207, 238
Laser fluence	~5 J/cm^2	Cooling gas (Ar)	16 l/min
Laser warm up	20 s	Auxilliary gas (Ar)	1.0 l/min
Ablation time	35 s	Sample gas (Ar)	0.9 l/min
Washout time	45 s	Carrier gas (He)	0.6 l/min

individual zircon grains of samples 48MR and 50MR providing results that are identical within error (Appendix A; B).

5. Results

In the following section, the morphology, internal structure and U–Pb ages of zircon grains in the four samples are described in order of increasing distance from the anorthosite intrusion. The CL and BSE images of the zircon grains usually show complementary features. Because the internal structures are more clearly visible in CL images, only these are presented (Fig. 3). The U–Pb isotope data and calculated ages for the analyzed zircon grains are listed in Appendix A, and illustrated in Figs. 4 and 5. The ages are also indicated on the corresponding CL zones (Fig. 3).

5.1. Quartzite 50MR

Zircon grains from this roof pendant quartzite sample are round to slightly elongate and sub- to anhedral. They are relatively small ranging from 150 to 250 μm. Most grains are colorless to light brown and composed of two zones: a CL-weak, sub-rounded core that is either featureless or shows a faint growth, sector or patchy zonation, and a highly luminescent rim that generally shows no internal structure in CL images. The boundaries between the two zones are straight as well as irregular and truncate the core zonation (Fig. 3a).

U–Pb dating of the cores provided a wide range of mostly concordant ages between 3.4 and 1.8 Ga (Figs. 3a, 4a, 5a). For the rims, two younger concordant age populations can be distinguished: one of ca. 950 Ma and a more dominant one of ca. 810 Ma. Few cores show discordance towards the cluster of younger ages found in the zircon rims (Fig. 4a).

Trace elements were analyzed in a few large enough zircon grains (Appendix B). The weakly luminescent cores show a large variation in the concentrations of the rare-earth elements (REE) with Lu_N/Gd_N ranging from 5 to 25. The younger (ca. 950 Ma and ca. 810 Ma) zircon domains have more tightly clustered REE abundances (Lu_N/Gd_N of 13 to 30). The cores display a relatively large variation in Th/U (0.2–1.7) compared to the narrow range in the younger age zones (0.2–0.7; Appendix B).

5.2. Quartzite 48MR

Zircon grains in this sample from the proximal contact aureole are relatively large (up to 500 μm) and are colorless to pink or light brown. Most grains are slightly elongate and euhedral and have three internal zones: (i) a CL-weak, rounded core that is either featureless or has faint growth, sector or patchy zonation, similar to sample 50MR, (ii) a luminescent mantle that typically shows no internal structure and, (iii) an oscillatory growth-zoned rim that imparts a euhedral shape to the grains (Fig. 3b). In some grains, however, only two zones are visible. These comprise either a low-luminescent core and a luminescent featureless rim or a highly luminescent core surrounded by a growth-zoned euhedral rim (Fig. 3b).

The weakly luminescent cores provide a range of old ages from ca. 3.3 to 1.8 Ga of which most (~75%) are concordant (Fig. 4c). In contrast, the strongly luminescent cores yielded a much younger

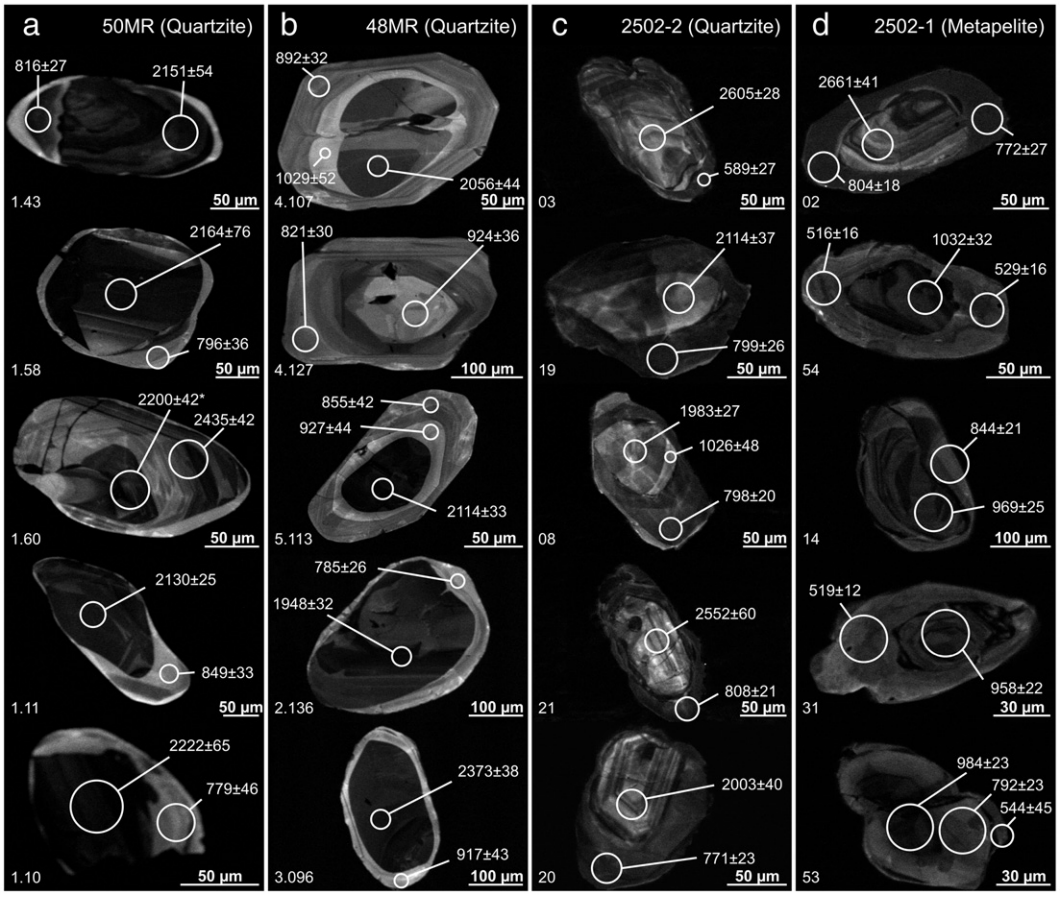

Fig. 3. Cathodoluminescence images of zircon grains from samples 50MR (a), 48MR (b), 2502–2 (c), and 2502–1 (d). Numbers to the lower left of grains indicate grain number. Ages younger than 1100 Ma are cited as $^{206}Pb/^{238}U$ ages, whereas for older zircon, the $^{207}Pb/^{206}Pb$ ages are given. Textural characteristics of zircon from quartzites within the anorthosite contact aureole (a, b) are similar (weakly luminescent, patchy or oscillatory-zoned cores having thin rims of higher luminescence). In contrast, zircon from the country rocks away from the anorthosite locality (c, d) is texturally variable and commonly shows volumetrically large rims.

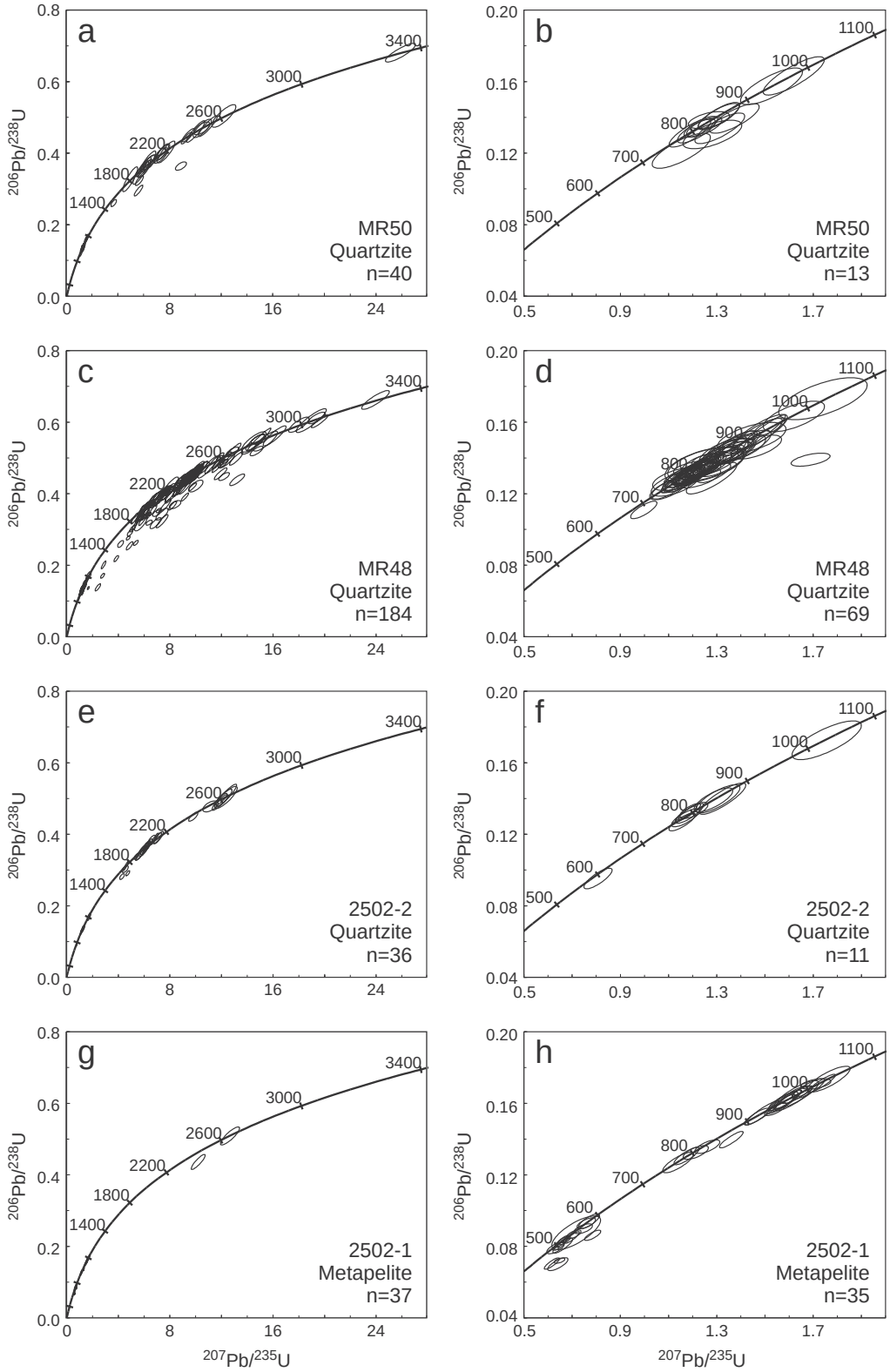

Fig. 4. Concordia diagrams showing the results of U–Pb analyses of zircon from samples 50MR (a, b), 48MR (c, d), 2502–2 (e, f), and 2502–1 (g–h). Zircon in quartzites from the contact aureole provided a relatively wide range of U–Pb ages, some of them showing discordance. Sample 2502–2 provides similar ages, but concordant results exclusively. Sample 2502–1 yielded young concordant ages and an additional age population at 490 to 590 Ma.

mean age of 955 ± 16 Ma. This early Neoproterozoic population is also found in the strongly luminescent mantles and rims of some grains. The growth-zoned rims that are moderately luminescent represent the youngest zone yielding a well-defined age of 810 ± 7 Ma (Figs. 3d, 4d, 5b).

Zircon grains in the sample were large enough to allow trace element measurements adjacent to spots used for U–Pb dating. The three zircon zones in the sample have distinct trace element characteristics. The weakly luminescent cores show a large variation in trace element concentrations including the REE (Lu_N/Gd_N = 7 to 32;

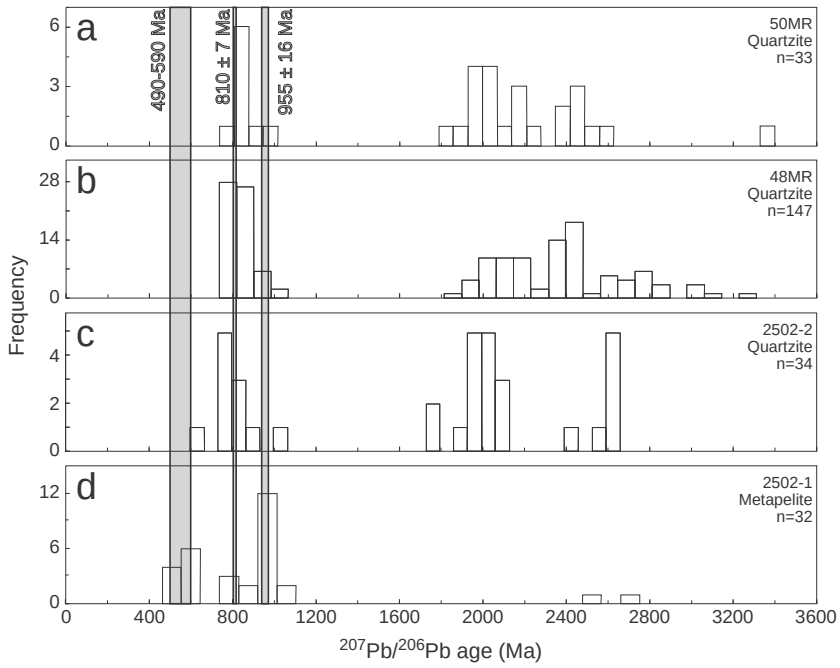

Fig. 5. Age histograms of $^{207}Pb/^{206}Pb$ age data from samples 50MR (a), 48MR (b), 2502–2 (c), and 2502–1 (d). Gray areas highlight the Neoproterozoic age populations that were identified in these samples. The similarities in zircon $^{207}Pb/^{206}Pb$ ages between quartzite samples from within the contact aureole (a, b) are illustrated. Although the results for the quartzite 2502–2 (c) are similar, the metapelite (d) shows a different age distribution.

Fig. 6a). They have variable negative to slightly positive Eu and positive Ce anomalies. In contrast, the younger (ca. 955 Ma and ca. 810 Ma) age domains have a narrower range of REE concentrations that overlap with those of the weakly luminescent cores (Fig. 6b). The 955-Ma zones have slightly higher REE abundances than the 810-Ma zones, but their Lu_N/Gd_N are similar (15.8 to 25.4 for 955-Ma zones and 12.6 to 22.4 for 810-Ma zones; Appendix B). Both younger zones consistently display negative Eu and positive Ce anomalies. The weakly luminescent cores show a large variation in Th/U (0.2–1.8) compared to the narrower range in the ca. 810-Ma zones (0.6–1.2). However, the largest spread in Th/U is found in the ca. 955-Ma zones (0.5–4.3; Fig. 7, Appendix B). Noteworthy is the fact that the discordant cores on average have twice the U concentrations (ca. 440 ppm) of the concordant ones (ca. 200 ppm; Appendix A; B).

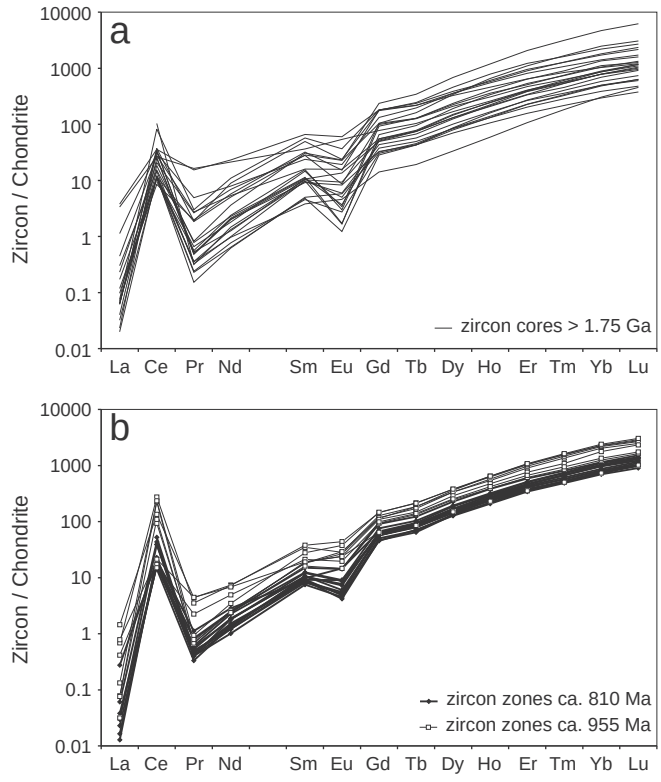

Fig. 6. Chondrite-normalized REE diagrams showing the REE content of detrital cores (a) and younger zircon zones (b) of sample 48MR. Chondrite values are after Taylor and McLennan (1985). The detrital zircon population shows a large variability in REE content, whereas zircon that yielded ages of ca. 955 Ma and, in particular, 810 Ma shows a narrow range of REE patterns.

5.3. Quartzite 2502–2

Most zircon grains in this quartzite sample, collected from the country rock far away from the anorthosite complex, are rounded to slightly elongate and have subhedral faces. Few grains are more elongate and euhedral. They have sizes between 150 and 200 μm and are either colorless or orange. The internal structures are complex consisting of up to four zones: (i) a rounded to elongate luminescent core with prominent growth or sector zoning (Fig. 3c), which furnish clusters of old concordant ages at ca. 2.6 Ga, 2.0 Ga and 1.75 Ga (Figs. 4e, f, 5c); (ii) a highly luminescent mantle of irregular thickness that (partly) surrounds some of the cores. These zones are commonly too narrow to be analyzed. One such zone could be dated and gave an age of ~1020 Ma, similar to the luminescent zones in zircon from the other quartzites (Fig. 3c); (iii) a low-luminescent homogeneous thick zone rimming the cores or mantles yielding a tightly clustered age of ca. 810 Ma; (iv) a thin CL-dark or -bright zone that usually rims one or more of the above zones and yielded ages of ca. 590 Ma (Fig. 3c).

5.4. Metapelite 2502–1

Zircon grains in the country-rock metapelite sample 2502–1 from outside the anorthosite contact aureole are elongate having subhedral crystal shapes. The average grain size ranges from 100 to 200 μm and

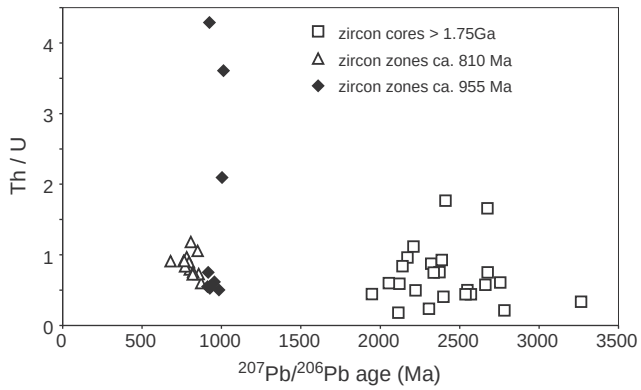

Fig. 7. Th/U versus $^{207}Pb/^{206}Pb$ age plot for different zircon age zones of sample 48MR. The detrital components show slight variation in Th/U. In contrast to the ca. 810 Ma zircon overgrowths, which show only minor variability in Th/U, ca. 955 Ma zircon shows a wide range of Th/U. This mostly reflects the relatively low U contents of this type of zircon.

the color ranges from orange or pink to colorless. In CL images, up to three zones can be identified in these grains (Fig. 3d): (i) a rounded core, displaying mostly oscillatory growth- or patchy zonation, having variable CL, and yielding ages between 1020 and 920 Ma with the exception of two that are much older at ca. 2.6 to 2.5 Ga (Figs. 3g, 5d); (ii) a weakly-luminescent wide zone rimming the cores, which is featureless or shows patchy zonation and is dated at ca. 810 Ma; (iii) featureless moderately-luminescent zones that are mostly thin and of variable shape and thickness, form rims around cores or the 810-Ma zones (Fig. 3d), and have late Neoproterozoic ages (590–490 Ma; Fig. 5d).

6. Discussion

6.1. Regional geological history

The weakly-luminescent rounded cores of zircon from the quartzites are characterized by a variety of relict zoning patterns, a wide range of old ages (3.4 to 1.8 Ga; Figs. 4, 5) and a large variation in trace element abundances (Fig. 6). Fine-scale growth zoning in some of these cores is interpreted to reflect a primary igneous character (e.g., Vavra, 1990; Hanchar and Miller, 1993), whereas sector zoning may be either indicative of an igneous growth history (Hanchar et al., 2001) or a metamorphic parentage (Watson and Liang, 1995). These characteristics of the cores indicate that they are of detrital origin. This is further supported by the fact that their internal structures are commonly truncated, which typically occurs as a result of mechanical abrasion during sediment transport. The 3.4 to 2.4 Ga zircon may have been derived from the Western and Eastern Dharwar cratons (e.g., Peucat et al., 1993; Jayananda et al., 2006), whereas the 1.8–2.0 Ga detrital zircon may have had sources in the Highland Complex of Sri Lanka (Braun and Kriegsman, 2003; Dobmeier and Raith, 2003). The lack of detrital zircon ages from metapelite sample 2502–1 reflects the fact that its protolith was deposited in a deep marine sedimentary environment where detrital zircon is rare. The three younger age populations i.e., at ca. 955 Ma, ca. 810 Ma and ca. 590–490 Ma are interpreted to be of metamorphic origin. These are discussed further in the following sections.

The intrusion of anorthosite into the sedimentary package and the accompanying contact metamorphism represents an important geological event in the Kadavur area. Unfortunately, the lack of zircon or other potentially datable minerals in the anorthosite does not allow direct determination of its emplacement age. Therefore, the timing of anorthosite emplacement has to be constrained from litho-structural relationships and U–Pb ages from the country rocks.

The oldest metamorphic event recorded by zircon in the country-rock quartzite and metapelite is of Grenville age (ca. 955 Ma). This early Neoproterozoic age domain is seen in zircon from all samples, clearly indicating that the ca. 955-Ma ages date a major episode of regional metamorphic zircon formation. Similar ages have been reported from the Madurai block (Santosh et al., 2003; Braun and Appel, 2006; Braun et al., 2007), which suggests that this part of the Southern Granulite Terrane together with the neighboring Eastern Ghats Belt (e.g., Simmat and Raith, 2008; Upadhyay et al., 2009) and the Wanni Complex of Sri Lanka (Braun and Kriegsman, 2003) underwent early Neoproterozoic HT metamorphism and igneous activity during Rodinia assembly. In the Kadavur area, relics of this earliest metamorphic event are preserved as bt + ky + Kfs + qtz + hem assemblages in the metapelites and as dynamically recrystallized quartz lenticules, kyanite pseudomorphs and ilmenite in the quartzites (Fig. 2c). In quartzites within the anorthosite contact aureole (50MR and 48MR), fabrics of Grenville age are extensively recrystallized to form a granoblastic aggregate of interlobate quartz grains (Fig. 2a, b). The static recrystallization can be related to contact heating during anorthosite intrusion. By implication, the anorthosite was emplaced after the early Neoproterozoic metamorphism, i.e., either at 810 Ma or 590–490 Ma.

Late Neoproterozoic (590–490 Ma) ages obtained from zircon rims of the country rocks cover the concordia from ca. 590 to 490 Ma. Although the number of analyses is small, two denser clusters can be observed at ca. 590 and 520 Ma (Fig. 4h). These ages correspond well to those obtained from rocks at Ayyarmalai, north of Kadavur (615 ± 11 and 529 ± 9 Ma; Raith et al., 2010) and are interpreted to represent renewed HT metamorphism during the Pan-African orogeny, the imprints of which are widespread throughout the Southern Granulite Terrane (e.g. Braun and Kriegsman, 2003; Ghosh et al., 2004). The youngest of these age clusters is well represented among gneisses of the Palghat Cauvery Shear Zone, possibly dating heating and decompression of the rocks during the collapse of the East African orogen (e.g., Clark et al., 2009). It is unlikely that the anorthosite was emplaced during this event, because Pan-African ages are not found in zircon from within the anorthosite contact aureole. Moreover, anorthosite bodies of such young age have not been reported thus far.

The 810 ± 7 Ma age population can be identified in all samples, but in contrast to the ca. 955-Ma age population, it is statistically more dominant in quartzites collected close to the anorthosite body (Fig. 5). This feature of the age spectrum is unlikely to be due to sampling bias or selective analyses, because care was taken to include zircon of all shapes, sizes and morphologies, and one spot per zircon zone was analyzed in all four samples. The combination between the prevalence of the ca. 810-Ma ages in the samples from the aureole and their strong static recrystallization fabric (due to contact heating) suggests that this age best approximates anorthosite emplacement and associated regional and contact metamorphism. Rapakivi granitoids closely associated with the Kadavur anorthosite in the wider Kadavur area have also been dated at ca. 0.8 Ga (e.g., Santosh et al., 2003; Ghosh et al., 2004; S. Brandt, pers. comm.). Such magmatic rock associations typically occur in Precambrian crystalline terranes, e.g., in the Proterozoic North Atlantic Shield orogen (e.g., Hubbard and Whitley, 1978; Ashwal, 1993; Moore et al., 1993), marking zones of crustal extension with increased heat input from the ascending asthenospheric mantle through a thinned continental lithosphere.

6.2. The U–Pb isotope and trace element systematics in metamorphosed zircon

The metapelite 2502–1 preserves a sil + bt + qtz paragenesis that did not cross the biotite-melting reaction. This is also the case for quartzite 2502–2 from the Sirumalai Ghats, where sil + bt + qtz is found in the thin metapelitic layers of the banded quartzites. The

occurrence of these mineral assemblages indicates that temperatures during the regional metamorphic events did not exceed 750 to 800 °C (Sengupta et al., 2009; Raith et al., 2010). In contrast, rocks from within the anorthosite contact aureole must have been exposed to significantly higher temperatures during magma intrusion and contact metamorphism. The almost mono-mineralic quartzites do not provide a mineral assemblage that could be used for thermometry. Titanium concentrations in zircon were analyzed, but due to the evident undersaturation for TiO_2 and the lack of a valid constraint on a_{TiO2} in these quartzites, Ti-in-zircon thermometry does not provide a reasonable peak T estimate for the intrusive event. The contrasting microtextures of the contact aureole and country rock quartzite (viz., strong static overprint in contact aureole quartzite vs. lack of it in the country rock quartzite) nevertheless suggests that the quartzite proximal to the anorthosite underwent significant contact metamorphism and hence must have experienced elevated temperature conditions.

Intrusion temperatures of anorthosites are estimated to be on the order of 1200 °C (e.g., Berg, 1977; Duchesne, 1984; Fuhrman and Lindsley, 1988; Ashwal, 1993; Markl et al., 1998; Westphal et al., 2003; Sengupta et al., 2008; Gleißner et al., 2010). Sample 50MR was taken from a quartzite outcrop surrounded by anorthosite. The observed field relations do not unambiguously establish whether the quartzite is a large xenolith within the anorthosite or represents an erosional remnant of a once continuous quartzite roof. In either case, quartzite in such close proximity to the anorthosite magma should have attained temperatures equal or close to that of the magma, independent of the heat transfer mechanism, i.e. temperatures of at least 1000 °C. For sample 48MR, which was taken from a quartzite ridge 600 m from the contact, T during contact metamorphism would have depended on the thermal state before intrusion, the distance to the contact, the thermal conductivity of the country rocks, and the efficiency of advective heat flow (e.g., Westphal et al., 2003). This is more difficult to estimate accurately, but models on conductive heat dissipation in such aureoles predict that, if the ambient T before emplacement was ca. 800 °C, crystalline rocks from ca. 600 m of the contact are estimated to have reached temperatures of ≥1000 °C within 5 Myr after the time of anorthosite intrusion (Westphal et al., 2003).

Based on the differences in thermal regimes affecting the rocks at the time of anorthosite emplacement, zircon from the samples can be divided into two groups: (1) zircon from country rock samples of the wider environs (samples 2502–1 and 2502–2), (2) zircon from quartzites within the contact aureole (48MR and 50MR).

6.2.1. Zircon in the country rocks of the wider environs

The textural characteristics of zircon grains from quartzite 2502–2 are different from those of quartzites from near the anorthosite in the following respects: (i) Detrital cores in zircon from quartzite 2502–2 commonly preserve their internal zonation, whereas zircon from quartzite in close proximity to the anorthosite are either featureless or show a faint growth, sector or patchy zonation (Fig. 3a,b,c). This may reflect different source rock characteristics, or could indicate a greater degree of recrystallization undergone by zircon from within the contact aureole due to the higher temperatures that were attained during contact heating; (ii) zircon in quartzite 2502–2 yielded ages between 590 and 490 Ma, which occur in very thin rims with growth zonation. These newly grown rims occur in many grains around zones having ages of ca. 810 Ma suggesting that this generation of zircon is omnipresent and dates a prominent late Neoproterozoic to Paleozoic zircon forming event. This age population is absent in zircon grains from quartzites within the contact aureole indicating that the contact aureole quartzites had very limited reactivity during the late Neoproterozoic event. This difference could have kinetic or kinematic causes. The quartzites of the contact aureole may have been entirely dehydrated during the earlier (ca. 810 Ma) contact metamorphism limiting the reactivity of the rocks. Alternatively, late Neoproterozoic zircon growth may have occurred in response to deformation from which the contact aureole quartzites were shielded by the competent anorthosite body.

Zircon grains from the biotite- and sillimanite-rich metapelite sample 2502–1 record a prominent Grenville age. In contrast to the quartzites, in which such ages occur exclusively in luminescent overgrowths, the Grenville ages in sample 2502–1 occur in growth-zoned low-luminescent cores (Fig. 3d). These cores reflect primary zircon growth during Grenville-age regional metamorphism, presumably as a product of prograde dehydration reactions. The widespread occurrence of volumetrically large zircon rims having ages of ca. 810 Ma or 590 to 490 Ma suggest a much higher reactivity of the metapelitic rocks compared to the quartzites. This difference in reactivity may be due to the release of fluids during dehydration of hydrous phases such as chlorite, muscovite, and biotite during prograde metamorphism in the metapelites and the essentially anhydrous nature of the quartzite.

6.2.2. Zircon in the contact aureole

Many detrital zircon cores from quartzites within the anorthosite contact aureole have rims that exhibit high luminescence and have uniform REE abundances. The rims are continuous and fully encapsulate the cores indicating that they formed in situ after the deposition of the sedimentary detritus. The rims provide concordant ages, show little or no internal structures, are poor in trace elements (e.g., U) relative to the cores, and are separated from these by convex interfaces (e.g., Fig. 3a, grain 1.58; Fig. 3b, grain 3.096). These characteristics suggest that the rims represent replacements of older, chemically unstable (i.e., metamict or internally strained) zircon (e.g., Pidgeon et al., 1998; Schaltegger et al., 1999; Rubatto et al., 2001; Geisler et al., 2007). Textures indicate that recrystallization involved an interface coupled replacement process, presumably through fluid assisted dissolution and reprecipitation (e.g., Fig. 3a, grain 1.43). The sub- to anhedral geometry of recrystallized zones is similar to—and appears inherited from—the detrital precursor reflecting the typical pseudomorphic nature of such replacement processes. In most grains the volumetric fraction of the recrystallized rims is small, suggesting only partial replacement. However, few grains lack detrital components and contain a luminescent core (e.g., Fig. 3b, grain 4.127), which could indicate that the replacement reaction locally went to completion. The U–Pb ages of the recrystallized zones provide a bimodal distribution of concordant ages. Mantles and cores comprising this type of zircon exclusively provide ca. 955-Ma ages, whereas rims of this type of zircon around cores yield ages of either ca. 955 Ma or 810 Ma. This shows that coupled dissolution–reprecipitation of zircon occurred both during the Grenville-age regional metamorphism and UHT contact metamorphism. The ca. 955-Ma zircon replacements show higher trace element content than recrystallized zones formed around 810 Ma. It is assumed that this reflects the difference in formation temperature and the depletion of the rocks during repetitive (U)HT metamorphism and extraction of REE-enriched fluids.

In addition to occurring as recrystallized rims that are highly luminescent and featureless, some of the ca. 810-Ma old zones in zircon from samples 50MR and 48MR show oscillatory growth zonation and remarkably well developed euhedral shapes (e.g., Fig. 3b, grain 4.107, 5.113). These zones are interpreted to represent newly grown zircon. Because no evidence of melting is observed in these rocks, this zircon is interpreted to have crystallized from fluids generated either by dehydration reactions occurring in the metapelites interlayered with the quartzites in response to contact heating, or by advective fluid flux into the contact aureole. The newly grown rims exclusively occur around high-luminescent cores or mantles. This shows that, in contrast to the detrital cores, the ca. 955-Ma zones were chemically stable and not susceptible to recrystallization during contact metamorphism. The chemical stability of these zones

relative to the detrital cores is presumably due to its low U contents (Appendix B) and young age, which would have caused only little radiation damage at the time of anorthosite magmatism and thus sustained relatively inert behavior at the ingress of fluids.

6.3. The robustness of the U–Pb chronometer in zircon under UHT conditions

The majority of the detrital cores (ca. 75%) preserve concordant ages (Fig. 4; Appendix A) despite being exposed to several episodes of HT metamorphism including the contact metamorphic UHT conditions of ≥1000 °C. This provides strong evidence that no significant Pb loss occurred from these domains and indicates that the T_c for Pb in zircon is even higher than previously estimated from experiments (950–1000 °C; Lee et al., 1997; Cherniak and Watson, 2001). Our results thus support the proposition made in earlier studies (e.g., Krogh, 1973; Mezger and Krogstad, 1997) that the loss of Pb from pristine zircon by volume diffusion is insignificant under crustal conditions and cannot be the cause of discordance of U-Pb ages.

Approximately 25% of the analyzed detrital zircon cores yielded a range of discordant ages (Fig. 4; Appendix A). It is unlikely that these analyses are the result of mixing of material from different age zones during laser ablation, because drilling into a different age zone results in a significant change in the isotope ratios during analysis. This is easily detectable by monitoring signal intensities and isotope ratios during an individual analysis. Analyses of some thin CL zones showing such anomalies were discarded. A mixed age can only remain unnoticed when equal amounts of the different zones are sampled throughout the analysis, the chances of which are quite small.

Below approximately 600 °C (e.g., Mezger and Krogstad, 1997), the recoil of α-particles and fission products of ^{235}U and ^{238}U decay damages the crystal structure of zircon leading to metamictization. Experimental studies have shown that Pb is relatively mobile and may be lost even from partially metamict zircon if the radiation-damaged zones are interconnected (e.g., McLaren et al., 1994; Geisler et al., 2002). At temperatures above 600 to 650 °C, the metamict domains get rapidly erased by structural recovery (Mezger and Krogstad, 1997). Some of the radiogenic Pb may become trapped in these domains, causing them to be discordant. The U concentrations in the discordant cores are on average a factor of two higher than in the concordant ones resulting in greater radiation damage in the former. This facilitates partial Pb loss from these domains upon annealing (Silver and Deutsch, 1963).

The annealing of radiation-damaged zircon may change local BSE and CL intensity (e.g., Nasdala et al., 2003; Nasdala et al., 2006). In our study, the discordant cores typically show a modified relict primary growth or sector zoning (e.g., compare Fig. 3b, grain 5.113 to Fig. 3a, b), reflecting the structural strain that was accommodated during annealing. In contrast to volume diffusion of Pb through crystalline grains, which produces 'smooth' age profiles from core to rim that can be described with an error function (e.g., McFarlane and Harrison, 2006; Kooijman et al., 2010), Pb loss associated with annealing is expected to only affect parts of single zircon zones having high U concentrations. The spatial resolution during laser ablation does not allow characterization of age heterogeneity within single zones. However, Flowers et al. (2010) clearly demonstrate heterogeneous Pb loss from annealed domains. Although interpreted differently, their age data and CL observations are consistent with the mechanisms described here.

The discordant core analyses define a discordia having a lower intercept age in the range of 1000 to 750 Ma, which suggests that Pb loss probably occurred during the HT metamorphic episodes at ca. 955 Ma and 810 Ma. It is noteworthy that only a small fraction of the analyses is discordant and the degrees of discordance are low, which indicates that most of the detrital zircon grains were pristine or were only weakly metamict. Our data confirm that volume diffusion of Pb through such pristine zircon lattices is insignificant, even at UHT metamorphic conditions, and does not cause significant discordance of U–Pb isotopes. This is consistent with experimental results that advocate a high T_c of Pb in zircon (Lee et al., 1997; Cherniak and Watson, 2001). In concurrence with the observations of Krogh (1973) and Mattinson (2005), discordance of zircon analyses is due to heterogeneous Pb loss from formerly metamict domains. Thus, the loss of Pb from zircon during (U)HT metamorphism only affects radiation-damaged crystals and results from temperature and fluid- or melt-assisted recrystallization and annealing. The results of this study thus provide an explanation for the success of the chemical abrasion technique developed by Mattinson (2005), which should promote dissolution of polycrystalline parts of zircons that formed by annealing of chemically unstable, metamict parts of individual zircon grains.

7. Conclusions

A large number of zircon cores from samples that underwent several episodes of HT metamorphism including UHT (≥1000 °C) contact metamorphism preserve concordant detrital ages, confirming that Pb loss by volume diffusion cannot be the dominant mechanism by which the U–Pb isotope systematics in zircon are disturbed. Discordance of some high-U cores can be attributed to entrapment of radiogenic Pb in these zones upon annealing. Textural evidence indicates that metamorphic rims around detrital cores are either new overgrowths crystallized during (U)HT metamorphism or completely re-equilibrated parts of detrital grains. The latter type of domains may have formed through recrystallization or fluid-assisted dissolution and reprecipitation processes. Such zircon provides concordant ages and is characterized by a higher structural or compositional stability. In addition to old U–Pb ages, detrital cores preserve a wide range of REE concentrations reflecting their heterogeneous provenance. Our study demonstrates that U–Pb- and REE systematics in pristine zircon are extremely robust to diffusive re-equilibration and provide reliable ages and genetic information in spite of their exposure to multiple HT and UHT metamorphic episodes.

Supplementary materials related to this article can be found online at doi: 10.1016/j.chemgeo.2011.09.013.

Acknowledgements

We thank P. Löbke for preparing the sample mounts and acknowledge M.A. Smit for helpful discussion and suggestions. We thank R.T. Pidgeon and an anonymous reviewer for their helpful comments on an earlier version of the manuscript. The elaborate, constructive reviews by J.M. Hanchar and F. Bussy, and the editorial handling by L. Reisberg are gratefully acknowledged. This project was funded by the German Research Foundation (DFG, ME 1717/18-1).

References

Ashwal, L.D., 1993. Anorthosites. Springer, Berlin, p. 422.
Ashwal, L.D., Tucker, R.D., Zinner, E.K., 1999. Slow cooling of deep crustal granulites and Pb-loss in zircon. Geochimica et Cosmochimica Acta 63, 2839–2851.
Bartlett, J.M., Dougherty-Page, J.S., Harris, N.B.W., Hawkesworth, C.J., Santosh, M., 1998. The application of single zircon evaporation and Nd model ages to the interpretation of polymetamorphic terrains: an example from the Proterozoic mobile belt of south India. Contributions to Mineralogy and Petrology 131, 181–195.
Baskar Rao, Y.J., Chetty, T.R.K., Janardhan, A.S., Gopalan, K., 1996. Sm–Nd and Rb–Sr ages and P–T history of the Archean Sittampundi and Bhavani layered meta-anorthosite complexes in Cauvery shear zone, South India: evidence for Neoproterozoic reworking of Archean crust. Contributions to Mineralogy and Petrology 125, 237–250.
Berg, J.H., 1977. Regional geobarometry in the contact aureoles of the anorthositic Nain Complex, Labrador. Journal of Petrology 18, 399–430.
Brandt, S., Schenk, V., Raith, M.M., Appel, P., Gerdes, A., Srikantappa, C., 2011. Late Neoproterozoic P–T evolution of HP-UHT granulites from the Palni Hills (South India): new constraints from phase diagram modeling, LA-ICP-MS zircon dating and in-situ EMP monazite dating. Journal of Petrology 52, 1813–1856.

Braun, I., Appel, P., 2006. U–Th-total Pb dating of monazite from orthogneisses and their ultra-high temperature metapelitic enclaves: implications for the multistage tectonic evolution of the Madurai Block, southern India. European Journal of Mineralogy 18, 415–427.
Braun, I., Kriegsman, L.M., 2003. Proterozoic crustal evolution of southernmost India and Sri Lanka. In: Yoshida, M., Windley, B.F., Dasgupta, S. (Eds.), Proterozoic East Gondwana: Supercontinent assembly and breakup: Geol. Soc. London Spec. Publ., 206, pp. 169–202.
Braun, I., Cenki-Tok, B., Paquette, J.-L., Tiepolo, M., 2007. Petrology and U–Th–Pb geochronology of the sapphirine-quartz-bearing metapelites from Rajapalayam, Madurai Block, Southern India: evidence for polyphase Neoproterozoic high-grade metamorphism. Chemical Geology 241, 129–147.
Chen, Y.D., Williams, I.S., 1990. Zircon inheritance in mafic inclusions from Bega Batholith granites, southeastern Australia: an ion microprobe study. Journal of Geophysical Research 95, 17787–17796.
Cherniak, D.J., Watson, E.B., 2001. Pb diffusion in zircon. Chemical Geology 172, 5–24.
Chetty, T.R.K., Bhaskar Rao, Y.J., 2006. The Cauvery Shear Zone, Southern Granulite Terrain, India: a crustal-scale flow structure. Gondwana Research 10, 77–85.
Chetty, T.R.K., Bhaskar Rao, Y.J., Narayana, B.L., 2003. A structural cross-section along Krishnagiri-Palani, southern granulite terrain, India. In: Ramakrishnan, M. (Ed.), Tectonics of Southern Granulite Terrain, Kuppam-Palani Geotransect. : Geol. Soc. India Memoir, 50, pp. 255–278.
Clark, C., Collins, A.S., Santosh, M., Taylor, R., Wade, B.P., 2009. The P–T–t architecture of a Gondwanan suture: REE, U–Pb and Ti-in-zircon thermometric constraints from the Palghat Cauvery shear system, South India. Precambrian Research 174, 129–144.
Corfu, F., Hanchar, J.M., Hoskin, P.W.O., Kinny, P., 2003. Atlas of zircon textures. In: Hanchar, H.M., Hoskin, P.W.O. (Eds.), Zircon. Mineral. Soc. Am., Rev. Mineral. Geochem., 53, pp. 469–500.
Dobmeier, C., Raith, M.M., 2003. Crustal architecture and evolution of the Eastern Ghats Belt and adjacent regions of India. In: Yoshida, M., Windley, B.F., Dasgupta, S. (Eds.), Proterozoic East Gondwana: Supercontinent assembly and breakup: Geol. Soc. London Spec. Publ., 206, pp. 169–202.
Dodson, M.H., 1973. Closure temperature in cooling geochronological and petrological systems. Contributions to Mineralogy and Petrology 40, 259–274.
Drury, S.A., Holt, R.W., 1980. The tectonic framework of the south Indian craton: a reconnaissance involving LANDSAT imagery. Tectonophysics 65, 1–15.
Drury, S.A., Harris, N.B.W., Holt, R.W., Reeves-Smith, G.J., Wightman, R.T., 1984. Precambrian tectonics and crustal evolution in south India. Journal of Geology 92, 3–20.
Duchesne, J.C., 1984. Massif anorthosites: another partisan review, in: (editor: Brown, W.S.), Feldspars, Feldspathoids and Their Parageneses. NATO Adv. Study Inst. Rennes, Reidel, pp. 411–433.
Flowers, R.M., Schmitt, A.K., Grove, M.J., 2010. Decoupling of U–Pb dates from chemical and crystallographic domains in granulite facies zircon. Chemical Geology 270, 20–30.
Fraser, G., Ellis, D., Eggins, S., 1997. Zirconium abundance in granulite-facies minerals, with implications for zircon geochronology in high-grade rocks. Geology 25, 607–610.
Fuhrman, M.L., Lindsley, D.H., 1988. Ternary-feldspar modeling and thermometry. American Mineralogist 73, 201–215.
Geisler, T., Pidgeon, R.T., van Bronswijk, W., Kurtz, R., 2002. Transport of uranium, thorium, and lead in metamict zircon under low-temperature hydrothermal conditions. Chemical Geology 191, 141–154.
Geisler, T., Schaltegger, U., Tomaschek, F., 2007. Re-equilibration of zircon in aqueous fluids and melts. Elements 3, 43–50.
Ghosh, J.G., de Wit, M.J., Zartman, R.E., 2004. Age and tectonic evolution of Neoproterozoic ductile shear zones in the Southern Granulite Terrain of India, with implications for Gondwana studies. Tectonics 23 (TC3006), 1–38.
Gleißner, P., Drüppel, K., Taubald, H., 2010. Magmatic evolution of anorthosites of the Kunene Intrusive Complex, NW Namibia: evidence from oxygen isotope data and trace element zoning. Journal of Petrology 51, 897–919.
Goldstein, S.L., Arndt, N.T., Stallard, R.F., 1997. The history of a continent from U–Pb ages of zircons from Orinoco River sand and Sm–Nd isotopes in Orinoco basin river sediments. Chemical Geology 139, 271–286.
Griffin, W.L., Powell, W.J., Pearson, N.J., O'Reilly, S.Y., 2008. GLITTER: data reduction software for laser ablation ICP-MS. In: Sylvester, P. (Ed.), Laser Ablation–ICP–MS in the Earth Sciences: Mineral. Assoc. Can. Short Course Series, 40, pp. 204–207.
Gulson, B.L., Krogh, T.E., 1973. Old lead components in the young Bergell Massif, south–east Swiss Alps. Contributions to Mineralogy and Petrology 40, 239–252.
Hanchar, J.M., Miller, C.F., 1993. Zircon zonation patterns as revealed by cathodoluminescence and back-scattered electron images: implications for interpretation of complex crustal histories. Chemical Geology 110, 1–13.
Hanchar, J.M., Finch, R.J., Hoskin, P.W.O., Watson, E.B., Cherniak, D.J., Mariano, A.N., 2001. Rare earth elements in synthetic zircon: Part 1. Synthesis, and rare earth element and phosphorus doping. American Mineralogist 86, 667–680.
Harley, S.L., Kelly, N.M., Möller, A., 2007. Zircon behaviour and the thermal histories of mountain chains. Elements 3, 43–50.
Harris, N.B.W., Santosh, M., Taylor, P.N., 1994. Crustal evolution in southern India: constraints from Nd isotopes. Journal of Geology 102, 139–150.
Harrison, T.M., Aleinikoff, J.N., Compston, W., 1987. Observations and controls on the occurrence of inherited zircon in Concord-type granitoids, New Hampshire. Geochimica et Cosmochimica Acta 52, 2549–2558.
Heaman, L., Parrish, R., 1991. U–Pb geochronology of accessory minerals. In: Heaman, L., Ludden, J.N. (Eds.), Applications of Radiogenic Isotope Systems to Problems in Geology: Min. Assoc. Canada, Short Course Handbook, pp. 59–102 (Ottawa).
Hoskin, P.W.O., Black, L.P., 2000. Metamorphic zircon formation by solid-state recrystallization of protolith igneous zircon. Journal of Metamorphic Geology 18, 423–439.
Hubbard, F.H., Whitley, J.E., 1978. Rapakivi granite, anorthosite and charnockitic plutonism. Nature 271, 439–440.
Jackson, S., Pearson, N.J., Griffin, W.L., Belousova, E.A., 2004. The application of laser ablation-inductively coupled plasma-mass spectrometry to in situ U–Pb zircon geochronology. Chemical Geology 211, 47–69.
Jayananda, M., Janardhan, A.S., Shivasubramanian, P., Percucat, J.J., 1995. Geochronologic and isotopic constraints on granulite formation in the Kodaikanal area, southern India. In: Yoshida, M., Santosh, M. (Eds.), India and Antarctica during Precambrian: Geol. Soc. India Memoir, 34, pp. 373–390.
Jayananda, M., Chardon, D., Peucat, J.J., Capdevila, R., 2006. 2.61 Ga potassic granites and crustal reworking in the western Dharwar craton, southern India: tectonic, geochronologic and geochemical constraints. Precambrian Research 150, 1–26.
Kooijman, E., Mezger, K., Berndt, J., 2010. Constraints on the U–Pb systematics of metamorphic rutile from *in situ* LA-ICP-MS analysis. Earth and Planetary Science Letters 293, 321–330.
Kooijman, E., Berndt, J., Mezger, K., in press. U–Pb dating of zircon by laser ablation ICP-MS: recent improvements and new insights. European Journal of Mineralogy
Krogh, T.E., 1973. A low-contamination method for hydrothermal decomposition of zircon and extraction of U and Pb for isotopic age determinations. Geochim. Cosmochim. Acta 37, 485–494.
Krogh, T.E., 1982. Improved accuracy of U–Pb zircon ages by the creation of more concordant systems using an air abrasion technique. Geochimica et Cosmochimica Acta 46, 637–649.
Lee, J.K.W., Williams, I.S., Ellis, D.J., 1997. Pb, U and Th diffusion in natural zircon. Nature 390, 159–162.
Ludwig, K.R., 2003. User's Manual for ISOPLOT/3.00: a geochronological toolkit for Microsoft Excel. Berkeley Geochronology Center Spec. Publ., 4, p. 71.
Markl, G., Frost, B.R., Bucher, K., 1998. The origin of anorthosites and related rocks from the Lofoten Islands, Northern Norway: I. Field relations and estimation of intrinsic variables. Journal of Petrology 39, 1425–1452.
Mattinson, J.M., 2005. Zircon U–Pb chemical abrasion ("CA-TIMS") method: combined annealing and multi-step partial dissolution analysis for improved precision and accuracy of zircon ages. Chemical Geology 220, 47–66.
McFarlane, C.R.M., Harrison, T.M., 2006. Pb-diffusion in monazite: constraints from a high-*T* contact aureole setting. Earth and Planetary Science Letters 250, 376–384.
McLaren, A.C., FitzGerald, J.C., Williams, I.S., 1994. The microstructure of zircon and its influence on the age determination from Pb/U isotopic ratios measured by ion microprobe. Geochimica et Cosmochimica Acta 58, 993–1005.
Meissner, B., Deters, P., Srikantappa, C., Köhler, H., 2002. Geological evolution of the Moyar, Bhavani and Palghat shear zones of southern India: implications for Gondwana correlation. Precambrian Research 114, 149–175.
Mezger, K., Krogstad, E.J., 1997. Interpretation of discordant U–Pb zircon ages: an evaluation. Journal of Metamorphic Geology 15, 127–140.
Moore, M., Davis, D.W., Robb, L.J., Jackson, M.C., Grobler, D.F., 1993. Archean rapakivi granite–anorthosite–rhyolite complex in theWitwatersrand basin hinterland, southern Africa. Geology 21, 1031–1034.
Nasdala, L., Pidgeon, R.T., Wolf, D., Irmer, G., 1998. Metamictization and U–Pb isotopic discordance in single zircons: a combined Raman microprobe and SHRIMP ion probe study. Mineralogy and Petrology 62, 1–27.
Nasdala, L., Zhang, M., Kempe, U., Panczer, G., Gaft, M., Andrut, M., Plötze, M., 2003. Spectroscopic methods applied to zircon. In: Hanchar, J.M., Hoskin, P.W.O. (Eds.), Zircon. Rev. Mineral. Geochem. : Mineral. Soc. Am., 53, pp. 427–467.
Nasdala, L., Kronz, A., Hanchar, J.M., Tichomirowa, M., Davis, D.W., Hofmeister, W., 2006. Effects of natural radiation damage on back-scattered electron images of single crystals of minerals. American Mineralogist 91, 1739–1746.
Nemchin, A.A., Giannini, L.M., Bodorkos, S., Oliver, N.H.S., 2001. Ostwald ripening as a possible mechanism for zircon overgrowth formation during anatexis: theoretical constraints, a numerical model, and its application to pelitic migmatites of the Tickalara Metamorphics, northwestern Australia. Geochimica et Cosmochimica Acta 65, 2771–2787.
Pan, Y., 1997. Zircon- and monazite-forming metamorphic reactions at Manitouwadge, Ontario. The Canadian Mineralogist 35, 105–118.
Peucat, J.J., Mahabaleswar, B., Jayananda, M., 1993. Age of younger tonalitic magmatism and granulitic metamorphism in the South Indian transition zone (Krishnagiri area); comparison with older Peninsular gneisses from the Gorur-Hassan area. Journal of Metamorphic Geology 11, 879–888.
Pidgeon, R.T., Nemchin, A.A., Hitchen, G.J., 1998. Internal structures of zircons from Archaean granites from the Darling Range batholith: implications for zircon stability and the interpretation of zircon U–Pb ages. Contributions to Mineralogy and Petrology 288–299.
Raith, M.M., Karmakar, S., Brown, M., 1997. Ultra-high-temperature metamorphism and multistage decompressional evolution of sapphirine granulites from the Palni Hill Ranges, southern India. Journal of Metamorphic Geology 15, 379–399.
Raith, M.M., Sengupta, P., Kooijman, E., Upadhyay, D., Srikantappa, C., 2010. Corundum-leucosome-bearing aluminous gneiss from Ayyarmalai, Southern Granulite Terrain, India: a textbook example of vapor phase-absent muscovite-melting in silica-undersaturated aluminous rocks. American Mineralogist 95, 897–907.
Rajesh, K.G., Chetty, T.R.K., 2006. Structure and tectonics of the Achankovil Shear zone, southern India. Gondwana Research 10, 86–98.
Roberts, M.P., Finger, F., 1997. Do U–Pb zircon ages from granulites reflect peak metamorphic conditions? Geology 25, 319–322.
Rubatto, D., Williams, I.S., Buick, I.S., 2001. Zircon and monazite response to prograde metamorphism in the Reynolds Range, central Australia. Contributions to Mineralogy and Petrology 140, 458–468.

Santosh, M., Collins, A.S., 2003. Gemstone mineralization in the Palghat-Cauvery Shear Zone systems (Karur-Kangayam Belt), southern India. Gondwana Research 6, 911–918.
Santosh, M., Yokoyama, K., Biju-Sekhar, S., Rogers, J.J.W., 2003. Multiple tectonothermal events in the granulite blocks of southern India revealed from EPMA dating: implications on the history of supercontinents. Gondwana Research 6, 29–63.
Santosh, M., Collins, A.S., Morimoto, T., Yokoyama, K., 2005. Depositional constraints and age of metamorphism in southern India: U–Pb chemical (EMPA) and isotopic (SIMS) ages from the Trivandrum Block. Geological Magazine 142, 1–14.
Schaltegger, U., Fanning, C.M., Gunther, D., Maurin, J.C., Schulmann, K., Gebauer, D., 1999. Growth, annealing and recrystallization of zircon and preservation of monazite in high-grade metamorphism: conventional and in-situ U–Pb isotope, cathodoluminescence and microchemical evidence. Contributions to Mineralogy and Petrology 134, 186–201.
Schärer, U., Corfu, F., Demaiffe, D., 1997. U–Pb and Lu–Hf isotopes in baddeleyite and zircon megacrysts from the Mbuji-Mayi kimberlite: constraints on the subcontinental mantle. Chemical Geology 143, 1–16.
Sengupta, P., Dasgupta, M., Dutta, N.R., Raith, M.M., 2008. Petrology across a calcareous rock-anorthosite interface from the Chilka Lake Complex, Orissa: implications for Neo-Proterozoic crustal evolution of the northern Eastern Ghats Belt. Precambrian Research 162, 40–58.
Sengupta, P., Dutta, U., Bhui, U.K., Mukhopadhyay, D., 2009. Genesis of wollastonite- and grandite-rich skarns in a suite of marble-calc-silicate rocks from Sittampundi, Tamil Nadu: constraints on the *P–T*-fluid regime in parts of the Pan-African mobile belt of South India. Mineralogy and Petrology 95, 179–200.
Silver, L.T., Deutsch, S., 1963. Uranium–lead isotopic variations in zircon: a case study. Journal of Geology 71, 721–758.
Simmat, R., Raith, M.M., 2008. U–Th–Pb monazite geochronometry of the Eastern Ghats Belt, India: Timing and spatial disposition of poly-metamorphism. Precambrian Research 162, 16–39.
Spear, F.S., 1999. Real-time AFM diagrams on your Macintosh. Geological Materials Research 1 (3), 1–19. http://gmr.minsocam.org.
Spear, F.S., Cheney, J.T., 1989. A petrogenetic grid for pelitic schists in the system SiO2–Al2O3–FeO–MgO–K2O–H2O. Contributions to Mineralogy and Petrology 101, 149–164.
Stacey, J.S., Kramers, J.D., 1975. Approximation of terrestrial lead isotope evolution by a two-stage model. Earth and Planetary Science Letters 26, 207–221.
Subramaniam, A.P., 1956. Petrology of the anorthosite–gabbro mass at Kadavur, Madras, India. Geological Magazine 93, 287–300.
Taylor, S.R., McLennan, S.M., 1985. The Continental Crust: Its Composition and Evolution. Blackwell Scientific, Oxford, p. 312.
Upadhyay, D., Gerdes, A., Raith, M.M., 2009. Unraveling sedimentary provenance and tectonothermal history of high temperature metapelites using zircon and monazite chemistry: a case study from the Eastern Ghats Belt, India. Journal of Geology 117, 665–683.
Vavra, G., 1990. On the kinematics of zircon growth and its petrogenetic significance: a cathodoluminescence study. Contributions to Mineralogy and Petrology 106, 90–99.
Vavra, G., Schmid, R., Gebauer, D., 1999. Internal morphology, habit and U–Th–Pb microanalysis of amphibolite to granuite facies zircon: geochronology of the Ivrea Zone (Southern Alps). Contributions to Mineralogy and Petrology 134, 380–404.
Watson, E.B., Liang, Y., 1995. A simple model for sector zoning in slowly grown crystals: implications for growth rate and lattice diffusion, with emphasis on accessory minerals in crustal rocks. American Mineralogist 80, 1179–1187.
Westphal, M., Schumacher, J.C., Boschert, M., 2003. High-temperature metamorphism and the role of magmatic heat sources at the Rogaland Anorthosite complex in southwestern Norway. Journal of Petrology 44, 1145–1162.
Wiedenbeck, M., Allé, P., Corfu, F., Griffin, W.L., Meier, M., Oberli, F., von Quadt, A., Roddick, J.C., Spiegel, W., 1995. Three natural zircon standards for U–Th–Pb, Lu–Hf, trace element, and REE analyses. Geostandard Newsletter 19, 1–23.
Williams, I.S., Buick, I.S., Cartwright, I.S., 1996. An extended episode of early Mesoproterozoic metamorphic fluid flow in the Reynolds Range, central Australia. Journal of Metamorphic Geology 14, 29–47.